

Seeing Through Pixel Motion: Learning Obstacle Avoidance from Optical Flow with One Camera

Yu Hu¹, Yang Zhang¹, Yunlong Song², Yang Deng¹, Feng Yu¹, Linzuo Zhang¹,
Weiyao Lin¹, Danping Zou^{1†}, and Wenxian Yu¹

Abstract—Optical flow captures the motion of pixels in an image sequence over time, providing information about movement, depth, and environmental structure. Flying insects utilize this information to navigate and avoid obstacles, allowing them to execute highly agile maneuvers even in complex environments. Despite its potential, autonomous flying robots have yet to fully leverage this motion information to achieve comparable levels of agility and robustness. Challenges of control from optical flow include extracting accurate optical flow at high speeds, handling noisy estimation, and ensuring robust performance in complex environments. To address these challenges, we propose a novel end-to-end system for quadrotor obstacle avoidance using monocular optical flow. We develop an efficient differentiable simulator coupled with a simplified quadrotor model, allowing our policy to be trained directly through first-order gradient optimization. Additionally, we introduce a central flow attention mechanism and an action-guided active sensing strategy that enhances the policy’s focus on task-relevant optical flow observations to enable more responsive decision-making during flight. Our system is validated both in simulation and the real world using an FPV racing drone. Despite being trained in a simple environment in simulation, our system demonstrates agile and robust flight in various unknown, cluttered environments in the real world at speeds of up to 6 m/s.

I. INTRODUCTION

Depth images, or depth maps, have long been useful in robotics, providing direct measurements of object distances, which are crucial for tasks like navigation and obstacle avoidance. Many existing planning and control algorithms can directly leverage the distance information in their task formulation, leading to straightforward implementation. Similarly, end-to-end control models, trained to map raw visual input directly to actions, have also been shown to benefit from explicit depth inputs, enhancing policy training and sim-to-real transfer [1], [2]. Depth sensing has thus enabled impressive achievements in navigation systems, including swarm navigation in complex environments such as forests [2]–[4].

While depth provides a structured and intuitive representation of the environment, it has limitations. Depth estimation from cameras, e.g., stereo cameras or a monocular camera with depth estimation algorithms, tends to suffer from reduced accuracy at greater distances, especially in outdoor environments where objects may be too far or lack sufficient features for reliable measurements. LIDAR, while offering precise depth data, is often too heavy and expensive for many lightweight or cost-sensitive applications, such as small drones.

[†] Corresponding author (dpzou@sjtu.edu.cn). ¹Shanghai Jiao Tong University. ²Y. Song is with University of Zurich.

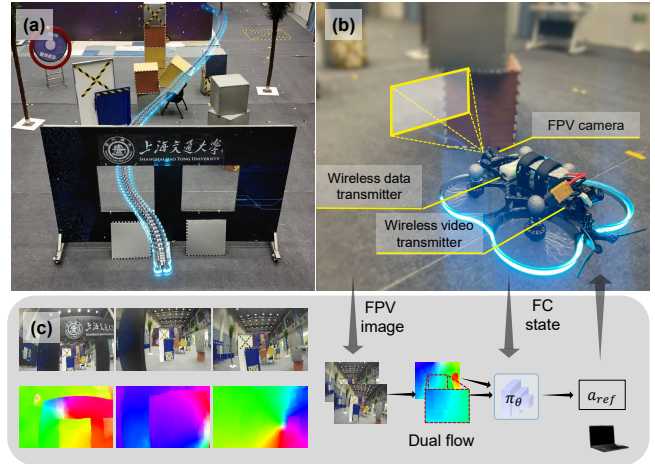


Fig. 1. Our drone autonomously navigates in the cluttered environment using optical flow estimated from a single camera. (a) Overview of the testing environment and trajectory. (b) Our real-world offboard is equipped with an FPV camera, a wireless video transmitter, and control system, a wireless data transmitter. (c) FPV images and optical flow estimations recorded during the flight.

Optical flow, in contrast, remains effective across a wider range of distances and provides valuable motion cues when depth perception is unreliable. It can also be computed using lightweight, low-cost monocular cameras, making it ideal for small aerial robots with limited payload and power capacity. Studies have shown that optical flow is fundamental to motion in flying insects, such as flies and bees, which rely primarily on monocular vision for navigation [5]. Despite having tiny heads and simple neural structures, insects effectively use optical flow for visual odometry [6], landing [7], measuring the gap [8], tunnel crossing [9], and obstacle avoidance [10]. This suggests that optical flow provides comprehensive information about self-motion and spatial layouts, showing its potential for autonomous flight. This natural reliance on visual cues motivates the question central to this work: *How can we enable autonomous flight using optical flow, without relying on explicit depth measurements?*

Leveraging optical flow for autonomous navigation in cluttered environments remains a fundamental challenge in robotics. First, optical flow estimation from images is prone to errors, especially in low-texture environments, varying illumination, and high-speed motions. Second, extracting essential motion cues, such as time-to-collision [11], nearness maps [12], and looming [13], remains an open problem, as existing algorithms rely on simplified assumptions like

pure translational motion or front-parallel obstacles. Third, designing effective control strategies based on these 2D cues is difficult due to the lack of intuitive metric information. Existing methods usually apply heuristic strategies such as braking [14], balancing the flow field [11], [15], and shifting to the side [13]. Such control strategies can lead to inferior control performance when the robot flies in complex environments at high speed. As a result, current flow-based methods are typically confined to controlled conditions and slow flight speeds (<3 m/s) [14].

Contribution: This work introduces a learning-based approach for flow-based monocular obstacle avoidance in quadrotors. Our method enables a high-performance FPV racing drone to navigate through complex, unstructured environments, such as forests, at high speeds, using only an onboard FPV camera for perception. The control policy is trained in simulation and then directly transferred to the real world zero shot. Our training environment features a simple point mass model for dynamics simulation and analytical gradient calculations. Additionally, we render a simple 3D scene that contains different obstacles, including planes, cuboids, spheres, and cylinders (Fig. 3). Existing methods typically rely on expensive high-fidelity simulators to generate realistic scenes, we discovered that our approach, despite its simplicity, can produce robust vision-based flight policies that generalize well to diverse real-world scenarios.

The key to our approach is a learning-based system that tightly merges robust flow estimation with an efficient policy optimization method using differentiable simulation. First, we use NeuFlow [16], a real-time, high-accuracy dense optical flow estimation method, to extract optical flow from image sequences. We also align the camera with the vehicle’s flight direction and enhance flow estimation using a central flow attention mechanism, allowing the system to focus on task-relevant flow information for downstream decision-making. Second, we optimize a memory-based control policy that maps the predicted optical flow to control commands. We use a first-order gradient optimization method, which provides stable training through low-variance policy gradients. Third, we develop a GPU-based differentiable simulation that provides ground-truth depth and optical flow using ray casting, achieving high-speed simulation. Our system is finally validated using an offboard setup, where video streams from the onboard camera are transmitted to a laptop for real-time processing and control. An overview of our system is given in Fig. 2.

II. RELATED WORK

A. Depth based Flight

Autonomous systems generally rely on constructing a 3D obstacle map using range sensors or structure from motion (SfM) algorithms. For instance, mapping-based approaches [17]–[20] generate an ESDF (Euclidean Signed Distance Field) map using depth sensors, which is then used for local path search and trajectory optimization. Other techniques simplify obstacle representation by focusing on

obstacle-free spaces [21]–[23], extracting safe flight corridors, and utilizing the convex hull properties of these corridors to simplify constrained trajectory optimization. Despite their successes, the modular pipeline introduces cumulative errors and added latency, which significantly hampers the vehicle’s performance, particularly during high-speed flight.

Learning-based methods aim to address these limitations by developing end-to-end planning or control policies. For instance, an imitation learning system [1] proposed to replace traditional mapping and planning with a neural network planner that directly converts depth images into collision-free trajectories, allowing the vehicle to navigate around obstacles. More recent work [2] employs an advanced first-order gradient optimization technique to train an end-to-end control policy, mapping depth inputs directly to control commands and enabling agile swarm flight in complex environments.

B. Optical Flow based Flight

There has been a sustained effort to integrate optical flow-based control into flying robot navigation [24]–[27]. Early studies focused predominantly on the optical flow flight control mechanisms observed in insects and attempted their adaptation to robotics. However, the mechanisms by which insects use optical flow in vision are highly complex. Insects can extract various motion cues from optical flow and employ different control strategies to navigate in 3D space [5]. For instance, bumblebees derive depth information from optical flow generated by translational motion to avoid obstacles [10] and assess gap sizes [10]. Locusts respond to looming visual stimuli [28] caused by impending collisions. Honeybees navigate corridors by balancing optical flow across different visual hemifields [9]. Fruit flies detect moving targets by processing regressive motion in optical flow [29].

Adapting these bio-inspired mechanisms to robotics is challenging, not only due to the diversity of the mechanisms themselves but also because of the difficulty in developing precise mathematical models or algorithms to replicate them. For example, time-to-collision [30] derived from flow divergence or looming motion cues is widely used in existing methods for collision avoidance. Two computational approaches are commonly used: one involves determining the Focus of Expansion [11], and the other involves calculating changes in relative size [31] [32]. The first approach only yields accurate results when the camera undergoes translational motion in static scenes and struggles with moving objects, while the second approach is effective only for fronto-parallel obstacles. Additionally, optical flow estimation is prone to errors due to the complexity of the scene and self-motion. A recent approach [25] attempted to improve flow-based control for flying robots by combining image features with optical flow, but this method has so far only been tested in controlled environments with printed textures, underscoring the ongoing gap between research and practical applications.

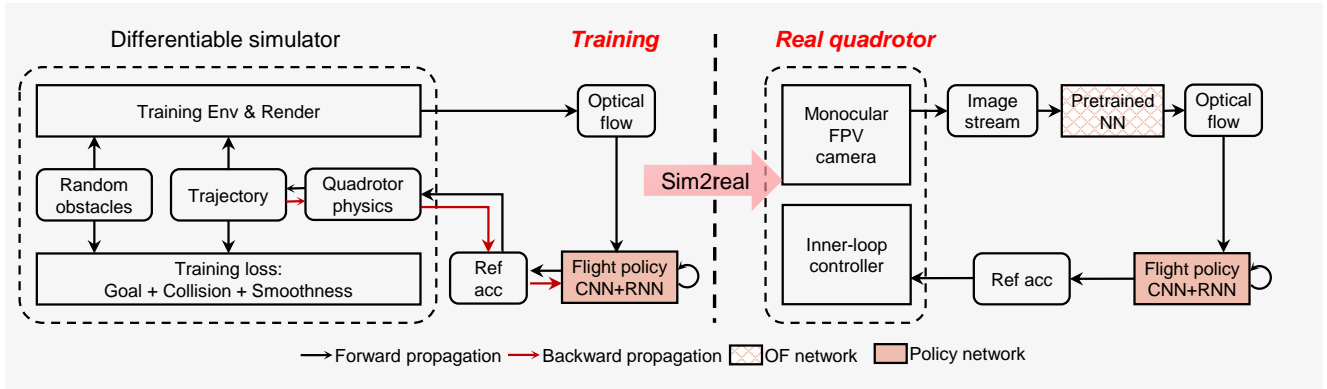


Fig. 2. **System overview.** We train our neural network policy using a differentiable simulator, which enables simulating quadrotor physics, rendering ground-truth optical flow, and calculating analytic policy gradients. We deploy our policy using a real FPV-style quadrotor in the real world. The reference acceleration output by the flight policy is sent into the inner-loop controller.

III. OPTICAL FLOW AS VISUAL CUES

Our goal is to achieve autonomous obstacle avoidance using a monocular camera that captures RGB images. While it is possible to directly use raw RGB images for learning navigation policies, employing optical flow as the visual input offers two main advantages. First, optical flow captures the relative 3D motion with respect to the environment, eliminating redundant information present in the RGB domain. As illustrated in Fig. 3, although the visual appearance (RGB images) in our training environment is very different from that of the actual deployment environments, these differences can be minimized in the flow domain. This small domain gap ensures the policy’s ability to transfer effectively from simulation to reality. Second, optical flow can be rendered in parallel at high speed by leveraging a simple geometric simulator, as shown in Fig. 3 (a). This approach is far more efficient and simpler than photorealistic RGB simulation, ensuring a time-efficient training process.

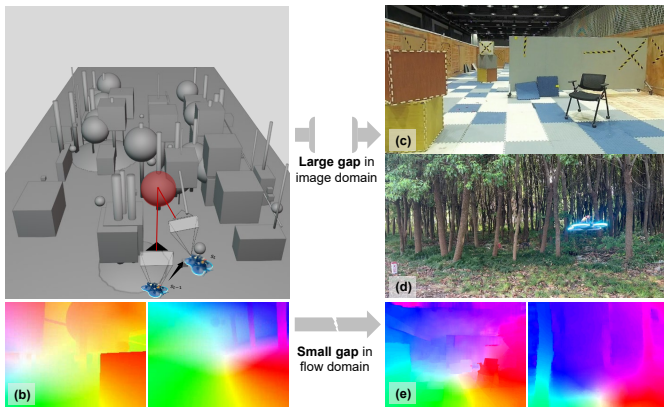


Fig. 3. **Our training environment vs Real-world testing environments.** (a) Our training environment features objects with simple geometric shapes. (b) Sampled ground-truth optical flow for training. (c-d) Real-world testing environments. (e) Estimated optical flow in the real world. Flow-based representation captures essential information about motion and removes redundant information that might be irrelevant for obstacle avoidance.

We briefly review the relationship between depth, optical

flow, and camera motion using the following equation:

$$\begin{bmatrix} \dot{\bar{p}}_x \\ \dot{\bar{p}}_y \end{bmatrix} = \frac{1}{p_{z_b}} \begin{bmatrix} -1 & 0 & \bar{p}_x \\ 0 & -1 & \bar{p}_y \end{bmatrix} b_{\mathbf{v}} + \begin{bmatrix} \bar{p}_x \bar{p}_{y_2} & -(1 + \bar{p}_x^2) & \bar{p}_y \\ 1 + \bar{p}_y^2 & -\bar{p}_x \bar{p}_y & -\bar{p}_x \end{bmatrix} b_{\omega}. \quad (1)$$

Here, \bar{p}_x , \bar{p}_y are the x and y displacement in image plane with unit of m. $b_{\mathbf{v}}$, b_{ω} are the linear velocity and angular velocity in the body frame. We formulate the flow using a pinhole camera model, assuming that the drone’s body frame coincides with the camera frame, where the forward direction aligns with the camera frame’s z-axis. The first part of the right-hand side can be referred to as the translational optical flow, as it is related to the ratio of velocity and depth. The second term on the right-hand side can be termed the rotational optical flow since it is solely associated with rotation.

The equation indicates that optical flow generated by translational motion encodes depth information about obstacles, increasing in magnitude as the drone approaches them. Therefore, a straightforward way to detect obstacles is by monitoring the flow magnitudes. However, this approach becomes unreliable when rotational motion is involved, as the flow caused by rotation contains no depth information. As shown in Fig. 4 (a) and (b), mistaking rotational flow for the evidence of approaching obstacles can result in false actions. This ambiguity renders traditional map-based planning methods inapplicable. Even if we manage to exclude the flow caused by rotation, the flow is less informative at the velocity projection point on image plane, also known as FoE (Focus of Expansion) where $[-1 \ 0 \ \bar{p}_x] b_{\mathbf{v}} = 0$ and $[0 \ -1 \ \bar{p}_y] b_{\mathbf{v}} = 0$. The depth information p_{z_b} is unobservable by optical flow at FoE, potentially causing insensitivity in the critical flight direction. Fig. 4 (c) and (d) show that in scenarios where 2-m-wide obstacle is positioned at distances of 6 m and 9 m, the optical flow near FoE exhibits similarity with small value, causing sensitivity to noise.

Therefore, utilizing optical flow for obstacle avoidance presents significant challenges, particularly due to the inher-

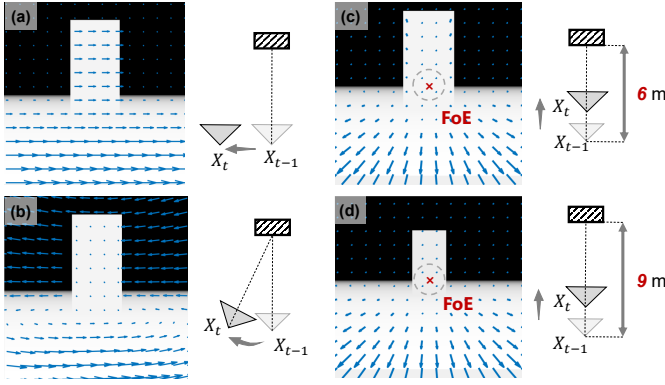


Fig. 4. **Challenges in detecting obstacles from optical flow.** **Left:** During rotation (b), the flow of obstacles can vanish, making it appear similar to the background flow in the pure translation scenario (a). **Right:** Flow values near the Focus of Expansion (FoE) are minimal, making it difficult to detect looming effects using local flow divergence with noisy estimation.

ent complexities of dense flow estimation from pixel motions and the additional difficulties posed by flow ambiguity. These factors make quadrotor trajectory planning and control in the optical flow domain highly challenging.

IV. METHOD

A. Problem Formulation

We formulate the quadrotor obstacle avoidance task as an optimization problem. The robot is modeled via a discrete-time dynamical system $x_{k+1} = f(x_k, u_k)$, characterized by continuous state and control input spaces, denoted as \mathcal{X} and \mathcal{U} , respectively. At each time step k , the system state is $x_k \in \mathcal{X}$, and the corresponding control input is $u_k \in \mathcal{U}$. We represent the quadrotor’s dynamics using a differentiable point-mass model with acceleration as the control input. The vehicle receives a cost signal $l_k(x_k, u_k)$ at each time step, which is used to evaluate the state and action. Additionally, the robot observes the environment through an RGB image o_k received from a monocular camera mounted on the vehicle.

We represent the control policy as a neural network $u_k = \pi_\theta(OF_k)$, which takes an optical flow OF_k as input and outputs the control input u_k . The objective of our optimization problem is to find the optimal policy parameters θ^* by minimizing the total loss via gradient descent:

$$\min_{\theta} \mathcal{L}_{\theta} = \sum_{k=0}^{N-1} l(x_k, u_k) = \sum_{k=0}^{N-1} l(x_k, \pi_{\theta}(OF_k)) \quad (2)$$

$$\theta \leftarrow \theta - \gamma \nabla_{\theta} \mathcal{L}_{\theta} \quad (3)$$

where γ is the learning rate. For policy training, we simulate ground-truth optical flow using our rendering engine. Given that we can only perceive the environment via an RGB camera, we use the NeuFlow [16] to estimate the optical flow $\hat{OF}_k = \text{NeuFlow}(o_k, o_{k-1})$ for real-world deployment. NeuFlow uses two consecutive images o_k and o_{k-1} captured by the camera. It is a state-of-the-art neural network architecture that achieves high-accuracy flow prediction and efficient inference on edge computing platforms.

B. Rendering Optical Flow

To render ground-truth optical flow for policy training, we implement a rendering engine. Given the current state, including position and orientation, of the vehicle, a ground-truth depth image is generated using ray tracing, where the 3D geometry of obstacles in the scene is solved to identify the intersection points along the rays. The nearest intersection point is then selected to determine the depth value for each pixel. To compute the optical flow at each time step OF_k , we use the depth image from the previous time step $Depth_{k-1}$ as a reference frame C_{k-1} . Each pixel (u_{k-1}, v_{k-1}) with its associated depth value $Depth_{k-1}$ is converted into a 3D point cloud. This point cloud is then reprojected onto the current image plane C_k , based on the drone’s state, to obtain the new pixel positions (u_k, v_k) . The ground truth optical flow OF_k is computed as $OF_k = (u_k - u_{k-1}, v_k - v_{k-1})_{2 \times h \times w}$. With our CUDA [33] parallelized implementation, our simulator achieves over 350 000 frames/s at a resolution of 48×64 on a single Nvidia RTX 3090 GPU. We utilize ultra-low resolution optical flow 12×16 as input to the policy network for two key reasons: 1) low-resolution flow enables more efficient training and deployment, and 2) downscaling a dense optical flow acts as a low-pass filter, preventing the policy from overfitting to irrelevant details.

C. Central Flow Attention with Active Sensing

While low-resolution optical flow offers several benefits, it might sacrifice important details. To address this, we introduce a central flow attention mechanism. Specifically, the central region of the original high-resolution optical flow is selected and downscaled; then, it is concatenated with the downscaled full flow to form a dual input for the control policy.

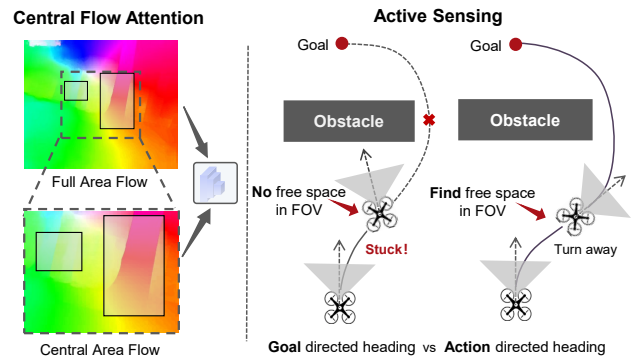


Fig. 5. We combine a central flow attention mechanism (left) with active sensing (right) to extract task-relevant flow information while maintaining efficient computation.

This concept is inspired by human pilots, who use eye gaze to concentrate on task-relevant visual information, e.g., the target gate, during drone racing [34]. This dual-resolution flow approach improves inference time by representing the optical flow of the entire image with a more compact matrix;

at the same time, it enhances focus on the image center, enabling the network to preserve crucial details in this region, leading to more precise decision-making.

For effective obstacle avoidance, we also combine flow estimation with active robot sensing. Specifically, the robot must maintain focus on its flight direction. However, due to the underactuated nature of the quadrotor, the camera may be oriented away from the desired view, such as facing backward. This misalignment, combined with the camera’s limited field of view, prevents the vehicle from perceiving obstacles in its path. To mitigate this, we actively align the camera with the direction of flight. An illustration of flow attention and active sensing is given in Fig. 5.

D. Policy Optimization via Differentiable Simulation

To optimize the control policy, we developed a high-performance simulator capable of simulating a point-mass model, a simplified yet effective representation of quadrotor dynamics, and rendering ground-truth depth and optical flow (Fig. 6). An important feature of our simulator is its ability to construct a computational graph that enables *automatic differentiation*, crucial for gradient-based policy optimization methods such as backpropagation, which is widely used for training neural networks. During the forward simulation, the vehicle’s trajectory is generated by randomly initializing the state of the vehicle and repeatedly applying the control commands output by the policy. Once the simulation completes, the computational graph is built. This allows us to apply Backpropagation Through Time (BPTT) to update the policy parameters efficiently by calculating gradients over the entire trajectory. The policy gradient can be expressed as $\partial \mathcal{L}_\theta / \partial \theta =$

$$\frac{1}{N} \sum_{k=0}^{N-1} \left(\sum_{i=0}^k \frac{\partial l_k}{\partial x_k} \prod_{j=i+1}^k \left(\frac{\partial x_j}{\partial x_{j-1}} e^{-\alpha \Delta t} \right) \frac{\partial x_i}{\partial \theta} + \frac{\partial l_k}{\partial u_k} \frac{\partial u_k}{\partial \theta} \right). \quad (4)$$

where α is an exponential decay of the dynamics gradients.

E. Loss Function

We define a navigation task where the objective is to follow a target velocity while avoiding obstacles. We formulate a loss function that has four terms: velocity tracking \mathcal{L}_v , obstacle avoidance \mathcal{L}_c , and control smoothness \mathcal{L}_a and \mathcal{L}_j . Specifically, the velocity tracking loss is defined as

$$\mathcal{L}_v = \frac{1}{T} \sum_{k=1}^T \text{Smooth L1}(\|v_k^{ref} - \bar{v}_k\|_2, 0) \quad (5)$$

where v_k^{ref} is the reference velocity and \bar{v}_k is the average velocity calculated via a moving average. We use an averaged speed instead of current speed to remove potential high-frequency oscillations, which has shown empirically better performance.

We define a collision avoidance loss as the following

$$\mathcal{L}_c = \frac{1}{T} \sum_{k=1}^T v_k^c \max(1 - (d_k - r_q), 0)^2 + \beta_1 \ln(1 + e^{\beta_2 (d_k - r_q)}),$$

where d_k represents the closest distance to the obstacle, r_q is the radius of the quadrotor, and v_k^c is the speed component directed towards the obstacle. The term v_k^c functions as an adaptive weight, dynamically adjusting the importance of proximity-based collision risk. If the agent is moving away from an obstacle, even when the distance is small, the risk is minimal. On the other hand, if the agent is approaching an obstacle at high speed, even when the obstacle is relative far, the risk can increase. The second term provides a soft and smooth penalty that ensures more robust obstacle avoidance, particularly in scenarios where obstacles are not immediately close but still pose a risk. Here, β_1 and β_2 are hyperparameters.

To avoid large oscillation in the action space, we define two smoothness losses to penalize the acceleration and jerk:

$$\mathcal{L}_a = \frac{1}{T} \sum_{k=1}^T \|a_k\|^2, \quad \mathcal{L}_j = \frac{1}{T-1} \sum_{k=1}^{T-1} \left\| \frac{a_k - a_{k+1}}{\Delta t} \right\|^2.$$

These losses help maintain a smoother flight, improving the quality of optical flow estimation and, hence, obstacle avoidance performance. The final loss is the weighted sum of these four terms, $L = \lambda_v \mathcal{L}_v + \lambda_c \mathcal{L}_c + \lambda_a \mathcal{L}_a + \lambda_j \mathcal{L}_j$, where $\lambda_v = 1, \lambda_c = 2, \lambda_a = 0.015, \lambda_j = 0.003$.

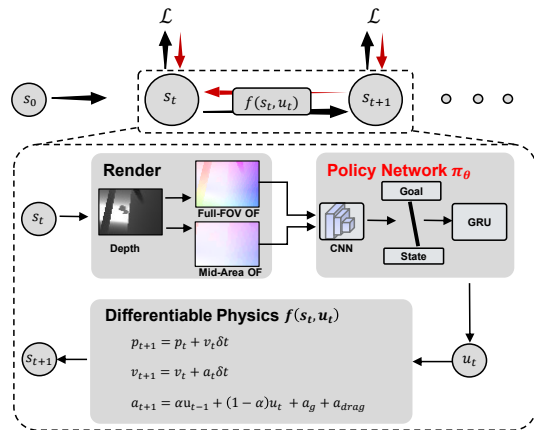


Fig. 6. **Overview of our differentiable simulator.** We use a point mass differentiable model for forward simulation (black arrow) and gradient calculation (red arrow). The controller response parameter is calibrated as $\alpha = e^{-\lambda(t-\tau)}$ where $\tau = \frac{2}{15}$ and $\lambda = 15$ in our platform.

V. EXPERIMENTS

A. Experiment Setup

We train our neural network control policy using our CUDA-based differentiable simulator (described in Sec. IV-D). Training on a standard computer equipped with an Intel i9 CPU and an Nvidia RTX 3090 GPU, the policy converges in approximately 2 hours. For real-world deployment, we build a lightweight FPV drone using off-the-shelf components together with a front-facing RGB camera. A unique feature of our system is its wireless data transmission capability, which sends digital images from the drone to a laptop equipped with Nvidia RTX 3070 GPU and receives control commands from the laptop for offboard control. This

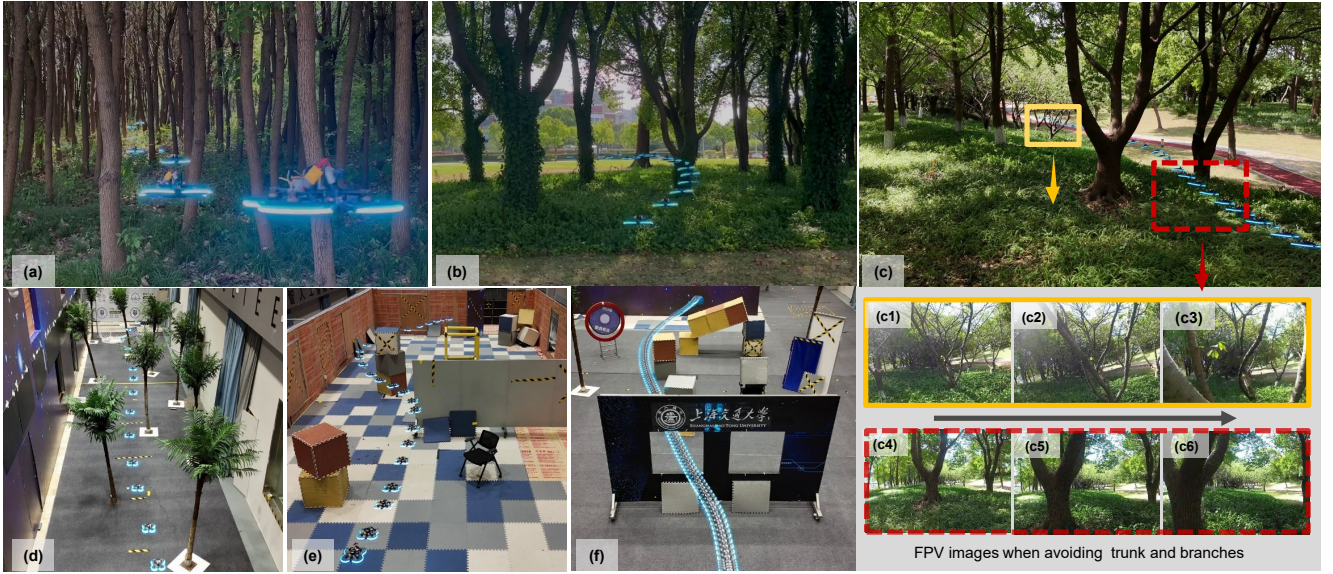


Fig. 7. **Real world experiment results.** We validate our algorithm in various unknown environments, including (a) dense forest, (b) sparse forest, (c) trees with branches, and cluttered indoor scenes (e) and (f). The quadrotor’s flight trajectory is visualized by overlaying its position in the video footage (please refer to the supplementary video for more details).

setup reduces the vehicle’s weight, enhancing both agility and flight duration.

B. Policy Training Performance

We demonstrate the effectiveness of our approach for policy training using differentiable simulation and optical flow in obstacle avoidance. We show that the introduced Central Flow Attention mechanism can significantly improve the convergence speed and asymptotic performance of the policy, shown in Fig. 8. With a smaller field of view (FOV), e.g., 90° , the flow naturally contains enough detailed information about obstacles in the environment; the central flow of attention allows marginal improvement. When using a large FOV, e.g., 150° , the captured image provides a broader environmental context but lack fine detail in specific regions, such as the flight path. In this case, the central optical flow offers crucial compensatory information, directing the control policy’s attention toward the most relevant features for navigation, and hence, improves the policy performance significantly.

We compare the performance of flow-based and depth-based policy training to highlight that learning to control from optical flow is a challenging task by definition. The learning curves are shown in Fig. 8. Depth image directly encodes the distance between the vehicle and obstacles, providing clear and actionable guidance for navigation. In contrast, optical flow offers more ambiguous information (illustrated via Fig. 4) as it represents motion rather than explicit distance. As a result, given only flow observations, a representation of the environment needs to be learned as part of learning control policies, making flow-based obstacle avoidance more challenging.

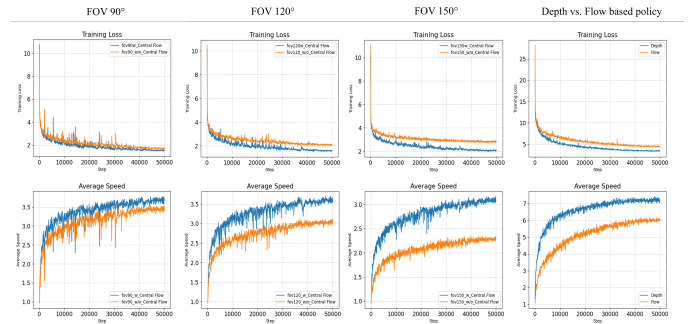


Fig. 8. **Training performance.** We verify the effectiveness of Central Flow Attention by comparing policies with or w/o the central flow under different camera FOV settings. The policy with Central Flow Attention mechanism (blue curve) has higher average speed and lower total loss, showing better performance. A comparison of depth-based policy and flow-based policy at high speed is shown at 4th column. The reference speed varies from 1.5 m/s to 15 m/s . The depth-based policy significantly outperforms the optical flow-based policy in terms of overall loss and average velocity in our training simulator.

C. Sim-to-Sim : A Baseline Comparison

This section studies the generalization capability of our flow-based policy in an unseen environment. Additionally, we compare the performance of our policy against state-of-the-art depth-based and mapping-based methods [1], [18]. We use a forest environment proposed in [1] and the Flightmare simulator [35] for evaluation. A top-down view of the forest environment is given in Fig. 9 (c). The results are shown in Fig. 9 (a), our flow-based policy successfully generalizes to the unseen forest environment without fine-tuning and achieves a high success rate at high speed, e.g., at 6 m/s compared to state-of-the-art depth-based learning methods. Notably, when using ground-truth optical flow, our policy achieved a 90% success rate even at speeds of 8 m/s . However, when utilizing the real-time lightweight

optical flow network, NeuFlow, the success rate dropped to 60%. This decline is attributed to the challenges posed by large displacement in optical flow during fast movement, which increases the error in optical flow estimation. These findings suggest that the current limitations in dense optical flow accuracy remain a constraint on our approach’s overall performance. Fig 9 (b) illustrates the velocity tracking performance, demonstrating that the policy is able to closely track and achieve velocities near the target speed while avoiding obstacles.

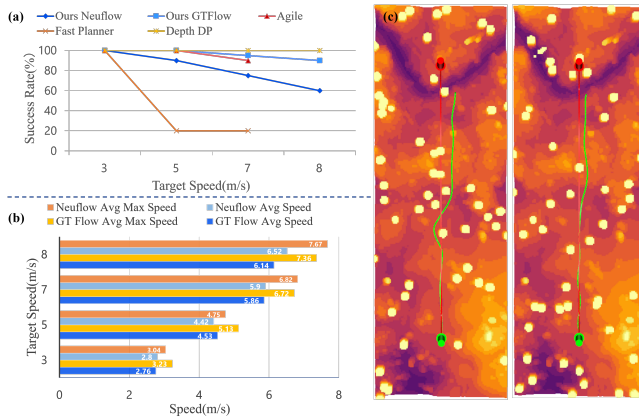


Fig. 9. **Baseline comparisons for sim-to-sim transfer.** We conducted 20 runs for each method. (a) success rates comparison of our algorithm and other SOTA methods in the same simulator with different target speeds. (b) velocity tracking performance. (c) visualization of the drone’s trajectories and the testing environments.

D. Sim-to-Real

We conduct extensive real-world experiments to demonstrate the strong generalization capability of our policy. Specifically, we test in a variety of environments (shown in Fig 7), including dense forests and cluttered indoor scenarios, featuring diverse obstacles such as thin branches, narrow gaps, walls, and chairs. Despite training our policy solely in a simple 3D environment with a point mass model, the policy transfers directly to these complex real-world settings in a zero-shot manner, achieving a maximum speed of 6 m/s. To the best of our knowledge, this represents one of the most agile flights achieved in complex real-world conditions using an RGB camera combined with optical flow estimation.

The strong generalization and agile flight performance of our system are attributed to both the accurate perception network and the robust control policy. The perception network (NeuFlow) provides real-time, relatively accurate optical flow predictions from captured images. Additionally, we combine these predictions with our proposed central flow attention mechanism and active sensing, allowing the robot to focus on its flight path while maintaining awareness of the broader environment. Furthermore, policy optimization using differentiable simulation enables end-to-end optimization of a control policy that maps optical flow directly to control commands via gradient-based optimization. This approach eliminates the need for human intuition, unlike traditional

rule-based or heuristic controllers, leading to more robust performance, particularly at high speeds where flow estimation becomes challenging due to large motion in the image.

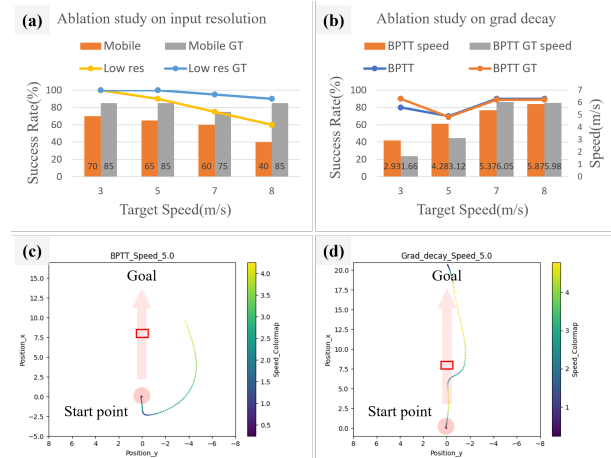


Fig. 10. **Ablation studies: flow resolution and gradient decay.**

E. Additional Studies

This section provides additional studies on the impact of optical flow resolution and the use of gradient decay for policy optimization, shown in Fig 10.

High-resolution vs Low-resolution Optical Flow: The default resolution of the optical flow for control is 12×16 . We experimented with a higher resolution of 96×128 using the MobileNet V3 architecture [36]. As shown in Fig. 10, increasing the optical flow resolution and using a deeper network did not yield significant improvements in obstacle avoidance performance. Interestingly, when ground-truth optical flow was used, MobileNet achieved a higher success rate, but it still performed worse than the lower-resolution input. This suggests that a smaller policy network with coarser interpolation offers greater robustness to errors introduced by flow estimation. Although ground-truth flow combined with a deeper network can encode more precise obstacle information, especially for small obstacles, the policy network tends to overfit the training environment, making it less robust to errors and diversity introduced by the optical flow estimation during real-world deployment.

Gradient Decay: Regarding the effectiveness of temporal gradient decay we use in policy gradient, we conducted tests in the simulation, with results as shown in the Fig 10. RNNs without gradient decay propagate gradients back through time. This leads to gradients being backpropagated to early actions where obstacles that have not yet been observed, causing the agent’s behavior to be overly conservative and even retreat from the initial state. Although the UAVs demonstrated a high success rate, their maximum speed significantly deviated from the desired speed. We treat this policy as not applicable in the real world. The function of gradient decay is to facilitate the appropriate propagation of gradients to adjacent frames, ensuring that our policy avoids obstacles within its observed range.

VI. CONCLUSION

This work introduces a learning-based method that achieves one of the most agile flow-based flights in natural environments using a monocular camera. Our real-world demonstrations indicate that optical flow is an effective representation for obstacle avoidance as it encodes valuable information about the vehicle motion and the surrounding environment. However, a performance gap remains between flow-based and depth-based navigation. This gap is attributed to the ambiguity of optical flow in representing obstacles, especially when rotational dynamics are included, and the need to learn a representation as part of the control policy. Future work could integrate state representation learning into differentiable-simulation-based policy training to provide explicit guidance for learning representations from optical flow observations.

REFERENCES

- [1] Antonio Loquercio, Elia Kaufmann, René Ranftl, Matthias Müller, Vladlen Koltun, and Davide Scaramuzza. Learning high-speed flight in the wild. *Science Robotics*, 6(59):eabg5810, 2021. Publisher: American Association for the Advancement of Science.
- [2] Yang Zhang, Yu Hu, Yunlong Song, Danping Zou, and Weiyao Lin. Back to newton’s laws: Learning vision-based agile flight via differentiable physics. 2024.
- [3] Xin Zhou, Xiangyong Wen, Zhepei Wang, Yuman Gao, Haojia Li, Qianhao Wang, Tiankai Yang, Haojian Lu, Yanjun Cao, Chao Xu, et al. Swarm of micro flying robots in the wild. *Science Robotics*, 7(66):eabm5954, 2022.
- [4] Xin Zhou, Zhepei Wang, Hongkai Ye, Chao Xu, and Fei Gao. Ego-planner: An esdf-free gradient-based local planner for quadrotors. *IEEE Robotics and Automation Letters*, 6(2):478–485, 2020. Publisher: IEEE.
- [5] Martin Egelhaaf. Optic flow based spatial vision in insects. *Journal of Comparative Physiology A*, 209(4):541–561, 2023.
- [6] Mandyam V Srinivasan, SW Zhang, M Lehrer, and TS Collett. Honeybee navigation en route to the goal: visual flight control and odometry. *Journal of Experimental Biology*, 199(1):237–244, 1996.
- [7] Emily Baird, Norbert Boeddeker, Michael R Ibbotson, and Mandyam V Srinivasan. A universal strategy for visually guided landing. *Proceedings of the National Academy of Sciences*, 110(46):18686–18691, 2013.
- [8] Sridhar Ravi, Olivier Bertrand, Tim Siesenop, Lea-Sophie Manz, Charlotte Doussot, Alex Fisher, and Martin Egelhaaf. Gap perception in bumblebees. *Journal of Experimental Biology*, 222(2):jeb184135, 2019.
- [9] Emily Baird and Marie Dacke. Visual flight control in naturalistic and artificial environments. *Journal of Comparative Physiology A*, 198:869–876, 2012.
- [10] Sridhar Ravi, Tim Siesenop, Olivier J Bertrand, Liang Li, Charlotte Doussot, Alex Fisher, William H Warren, and Martin Egelhaaf. Bumblebees display characteristics of active vision during robust obstacle avoidance flight. *Journal of Experimental Biology*, 225(4):jeb243021, 2022.
- [11] Kahlouche Souhila and Achour Karim. Optical flow based robot obstacle avoidance. *International Journal of Advanced Robotic Systems*, 4(1):2, 2007.
- [12] Olivier JN Bertrand, Jens P Lindemann, and Martin Egelhaaf. A bio-inspired collision avoidance model based on spatial information derived from motion detectors leads to common routes. *PLoS computational biology*, 11(11):e1004339, 2015.
- [13] Jiannan Zhao, Cheng Hu, Chun Zhang, Zhihua Wang, and Shigang Yue. A bio-inspired collision detector for small quadcopter. In *2018 International Joint Conference on Neural Networks (IJCNN)*, pages 1–7. IEEE, 2018.
- [14] Feng Xiao, Peter Zheng, Julien Di Tria, Basaran Bahadır Kocer, and Mirko Kovac. Optic flow-based reactive collision prevention for mavs using the fictitious obstacle hypothesis. *IEEE Robotics and Automation Letters*, 6(2):3144–3151, 2021.
- [15] Rik J Bouwmeester, Federico Paredes-Vallés, and Guido CHE De Croon. Nanoflownet: Real-time dense optical flow on a nano quadcopter. In *2023 IEEE International Conference on Robotics and Automation (ICRA)*, pages 1996–2003. IEEE, 2023.
- [16] Zhiyong Zhang, Huaizu Jiang, and Hanumant Singh. Neuflow: Real-time, high-accuracy optical flow estimation on robots using edge devices. *arXiv preprint arXiv:2403.10425*, 2024.
- [17] Boyu Zhou, Jie Pan, Fei Gao, and Shaojie Shen. Raptor: Robust and perception-aware trajectory replanning for quadrotor fast flight. *IEEE Transactions on Robotics*, 37(6):1992–2009, 2021.
- [18] Boyu Zhou, Fei Gao, Luqi Wang, Chuhao Liu, and Shaojie Shen. Robust and efficient quadrotor trajectory generation for fast autonomous flight. *IEEE Robotics and Automation Letters*, 4(4):3529–3536, 2019.
- [19] Helen Oleynikova, Zachary Taylor, Marius Fehr, Roland Siegwart, and Juan Nieto. Voxblox: Incremental 3d euclidean signed distance fields for on-board mav planning. In *IEEE/RSJ International Conference on Intelligent Robots and Systems (IROS)*, 2017.
- [20] Luxin Han, Fei Gao, Boyu Zhou, and Shaojie Shen. Fiesta: Fast incremental euclidean distance fields for online motion planning of aerial robots. In *2019 IEEE/RSJ International Conference on Intelligent Robots and Systems (IROS)*, pages 4423–4430, 2019.
- [21] Yunfan Ren, Fangcheng Zhu, Wenyi Liu, Zhepei Wang, Yi Lin, Fei Gao, and Fu Zhang. Bubble planner: Planning high-speed smooth quadrotor trajectories using receding corridors. In *2022 IEEE/RSJ International Conference on Intelligent Robots and Systems (IROS)*, pages 6332–6339, 2022.
- [22] Jesus Tordesillas, Brett T. Lopez, Michael Everett, and Jonathan P. How. FASTER: Fast and safe trajectory planner for navigation in unknown environments. *IEEE Transactions on Robotics*, 38(2):922–938, 2022.
- [23] Jesus Tordesillas and Jonathan P How. MADER: Trajectory planner in multi-agent and dynamic environments. *IEEE Transactions on Robotics*, 2021.
- [24] Julien R Serres and Franck Ruffier. Optic flow-based collision-free strategies: From insects to robots. *Arthropod structure & development*, 46(5):703–717, 2017.
- [25] Guido Croon, Christophe De Wagter, and Tobias Seidl. Enhancing optical-flow-based control by learning visual appearance cues for flying robots. *Nature Machine Intelligence*, 3:33–41, 01 2021.
- [26] Guido C H E de Croon. Monocular distance estimation with optical flow maneuvers and efference copies: a stability-based strategy. *Bioinspiration & Biomimetics*, 11(1):016004, jan 2016.
- [27] Guido Croon, Julien Dupeyroux, Christophe De Wagter, Abhishek Chatterjee, Diana Olejnik, and Franck Ruffier. Accommodating unobservability to control flight attitude with optic flow. *Nature*, 610:485–490, 10 2022.
- [28] Nicholas Hatsopoulos, Fabrizio Gabbiani, and Gilles Laurent. Elementary computation of object approach by a wide-field visual neuron. *Science*, 270(5238):1000–1003, 1995.
- [29] Francisco Zabala, Peter Polidoro, Alice Robie, Kristin Branson, Pietro Perona, and Michael H Dickinson. A simple strategy for detecting moving objects during locomotion revealed by animal-robot interactions. *Current Biology*, 22(14):1344–1350, 2012.
- [30] Randal C. Nelson and Jhon Aloimonos. Obstacle avoidance using flow field divergence. *IEEE Transactions on pattern analysis and machine intelligence*, 11(10):1102–1106, 1989.
- [31] Berthold KP Horn, Yajun Fang, and Ichiro Masaki. Time to contact relative to a planar surface. In *2007 IEEE intelligent vehicles symposium*, pages 68–74. IEEE, 2007.
- [32] Gengshan Yang and Deva Ramanan. Upgrading optical flow to 3d scene flow through optical expansion. In *Proceedings of the IEEE/CVF Conference on Computer Vision and Pattern Recognition*, pages 1334–1343, 2020.
- [33] NVIDIA, Péter Vingelmann, and Frank H.P. Fitzek. Cuda, release: 10.2.89, 2020.
- [34] Christian Pfeiffer and Davide Scaramuzza. Human-piloted drone racing: Visual processing and control. *IEEE Robotics and Automation Letters*, 6(2):3467–3474, 2021.
- [35] Yunlong Song, Selim Naji, Elia Kaufmann, Antonio Loquercio, and Davide Scaramuzza. Flightmare: A flexible quadrotor simulator. In *Proceedings of the 2020 Conference on Robot Learning*, pages 1147–1157, 2021.
- [36] Andrew Howard, Mark Sandler, Bo Chen, Weijun Wang, Liang-Chieh Chen, Mingxing Tan, Grace Chu, Vijay Vasudevan, Yukun Zhu, Ruoming Pang, Hartwig Adam, and Quoc Le. Searching for mobilenetv3. In *2019 IEEE/CVF International Conference on Computer Vision (ICCV)*, pages 1314–1324, 2019.